Predicted Efficiency of a Low-Temperature Nanofluid-Based Direct Absorption Solar Collector

Himanshu Tyagi
School of Mechanical, Aerospace, Chemical and Materials Engineering,
Arizona State University,
Tempe, AZ 85287-6106

Patrick Phelan[1]
School of Mechanical, Aerospace, Chemical and Materials Engineering,
National Center of Excellence on SMART Innovations,
Arizona State University,
Tempe, AZ 85287-6106
e-mail: phelan@asu.edu

Ravi Prasher
Adjunct Professor
School of Mechanical, Aerospace, Chemical and Materials Engineering,
Arizona State University,
Tempe, AZ 85287-6106

Due to its renewable and nonpolluting nature, solar energy is often used in applications such as electricity generation, thermal heating, and chemical processing. The most cost-effective solar heaters are of the "flat-plate" type, but these suffer from relatively low efficiency and outlet temperatures. The present study theoretically investigates the feasibility of using a nonconcentrating direct absorption solar collector (DAC) and compares its performance with that of a typical flat-plate collector. Here a nanofluid—a mixture of water and aluminum nanoparticles—is used as the absorbing medium. A two-dimensional heat transfer analysis was developed in which direct sunlight was incident on a thin flowing film of nanofluid. The effects of absorption and scattering within the nanofluid were accounted for. In order to evaluate the temperature profile and intensity distribution within the nanofluid, the energy balance equation and heat transport equation were solved numerically. It was observed that the presence of nanoparticles increases the absorption of incident radiation by more than nine times over that of pure water. According to the results obtained from this study, under similar operating conditions, the efficiency of a DAC using nanofluid as the working fluid is found to be up to 10% higher (on an absolute basis) than that of a flat-plate collector. Generally a DAC using nanofluids as the working fluid performs better than a flat-plate collector, however, much better designed flat-plate collectors might be able to match or outperform a nanofluids based DAC under certain conditions. [DOI: 10.1115/1.3197562]

1 Introduction

Several types of solar collectors have been used to harness solar energy. The most common of these are the flat-plate black-surface absorbers, which absorb solar energy through a solid surface [1]. However these types of solar collectors exhibit several shortcomings, such as limitations on incident flux density, relatively high heat losses, and corrosion effects. In order to overcome the drawbacks of these solid-surface collectors attempts have been made to use black liquids (such as water soluble dyes) as the absorbing medium [2]. Such a design enables the solar receiver to withstand much higher incident fluxes and thus produce higher outlet temperatures. Recently work was reported to extend the concept of direct radiative absorption by a conventional fluid to particle-laden-fluids. Both experimental [3] and numerical models [4–6] were presented to assess the feasibility of such a collector. The advantage of using a particle-laden-fluid is that due to the presence of the small particles, scattering of incident radiation takes place, which can lead to increased radiative absorption, and hence an enhancement in collector efficiency. Therefore, in order to properly design a particle-fluid-based solar collector it is important to develop a basic understanding of the radiative properties of particle-laden fluids.

The application of nanofluids as a working medium for solar collectors is a relatively new concept. Due to their small size and physical properties a comprehensive analysis of radiative heat transfer of nanofluids is inherently complex. In some recent studies aspects of this complex physics have been addressed [7,8]. Furthermore, the addition of nanoparticles to a base fluid has been shown to enhance other physical properties of the fluid as well, such as thermal conductivity [9–12] and mass diffusivity [13]. The overall use of nanofluids in various heat transfer applications has been reviewed in Ref. [14].

The objective of this study is to compare the efficiency of a direct absorption solar collector (DAC), using a nanofluid as the absorbing medium, to that of a conventional flat-plate collector. The nanofluid consists of water with aluminum nanoparticles. As part of this study, a two-dimensional heat transfer model was prepared and solved numerically. The model accounted for the incident sunlight and included the effects of absorption and scattering by the working medium. The energy balance equation and heat transport equation were solved numerically in MATLAB. Lastly, the collector efficiencies were evaluated for various conditions. It was observed that the efficiency of a nanofluid DAC is a function of various geometrical parameters and operating conditions. Under comparable operating conditions, the collector efficiency of a nanofluid DAC was found to be higher than that of a flat-plate type collector using a conventional working fluid.

2 Theoretical Model

The schematic of the nanofluid-based direct absorption solar collector is shown in Fig. 1. The fluid is contained within the enclosed space of the DAC. The bottom wall is considered to be adiabatic, i.e., no heat flux is allowed to pass through it, except for transmitted radiation. This assumption is based on the case when the bottom surface is highly insulating and transparent. The fluid is enclosed at the top by a glass surface, which allows most of the incident solar flux to pass through. This top surface is assumed to be exposed to the ambient atmosphere and thus loses heat by

[1]Corresponding author.

Contributed by the Solar Energy Engineering Division of ASME for publication in the JOURNAL OF SOLAR ENERGY ENGINEERING. Manuscript received July 11, 2007; final manuscript received September 24, 2008; published online September 17, 2009. Review conducted by Rainer Tamme. Paper presented at the 2007 ASME Solar Energy Division and Advanced Energy Systems Division Conference (ES2007), Long Beach, CA, June 27–29, 2007.

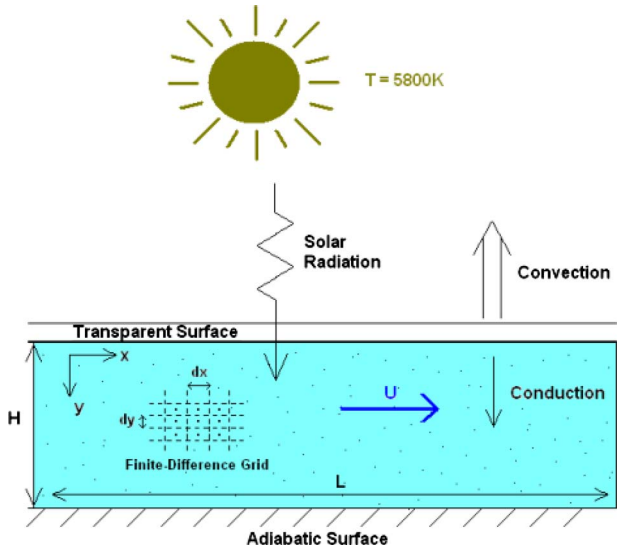

Fig. 1 Schematic of the nanofluid-based direct absorption solar collector

convection. In order to model the heat transfer characteristics of this surface it is assumed that it loses heat to the ambient through convection.

The incident radiation is considered to be the incoming solar radiation. For the study of the principal behavior of the nanofluid-based DAC, atmospheric absorption was neglected in these calculations. Hence, the incident solar intensity is calculated using the blackbody relation given by Eq. (1), where the value of T_{solar} is taken as 5800 K:

$$I_{b\lambda}(\lambda, T_{\text{solar}}) = \frac{2hc_o^2}{\lambda^5\left[\exp\left(\frac{hc_o}{\lambda k_B T_{\text{solar}}}\right) - 1\right]} \tag{1}$$

In this equation h is Planck's constant, k_B is the Boltzmann constant, c_o is the speed of light in vacuum, and λ is the wavelength. Using this relation the spectral intensity incident on the solar collector was evaluated. The radiation intensity within the fluid was assumed to vary only in one dimension (along the y-direction). Equation (2) is the radiative transport equation, which was used in this model. The right side of the equation determines the attenuation in the intensity as the radiation travels through the fluid

$$\frac{\partial I_\lambda}{\partial y} = -(K_{a\lambda} + K_{s\lambda})I_\lambda = -K_{e\lambda}I_\lambda \tag{2}$$

where $K_{a\lambda}$ is the spectral absorption coefficient, and $K_{s\lambda}$ the spectral scattering coefficient. Taken together they can also be represented as $K_{e\lambda}$, the spectral extinction coefficient. Since the temperatures in the solar collector are not expected to be very high, the *emission* term has not been included in Eq. (2). Also, in order to keep the model simple, the effect of *in-scattering* has not been considered. As will be described later in Eqs. (7*a*)–(7*c*), the scattering efficiency varies as the fourth power of particle size, and the absorption efficiency varies almost linearly with the particle size, therefore, this simplification is justified for calculations involving nanoscale particles.

For pure fluids, scattering can be neglected and only the attenuation caused by absorption may be considered. For that case, the spectral absorption coefficient can be calculated using Eq. (3)

$$K_{a\lambda} = \frac{4\pi\kappa}{\lambda} \tag{3}$$

where κ is the index of absorption. However, for nanofluids, where the presence of small particles influences the nature of absorption, as well as scattering, some complex relationships need to be used. Since in the present problem the particles have a mean diameter of about 5 nm, the approximation of Rayleigh scattering [15] can be applied. This approximation is valid when $\alpha \ll 1$ and $|m|\alpha \ll 1$, where α is defined as the size parameter and is given by

$$\alpha = \frac{\pi D}{\lambda} \tag{4}$$

where D is the diameter of the particles, and $m(=n+i\kappa)$ is defined as the normalized refractive index of the particles

$$m = \frac{m_{\text{particles}}}{n_{\text{fluid}}} \tag{5}$$

In physical terms, Rayleigh scattering can be understood as the regime in which the particle size is much smaller than the wavelength of the incident radiation. In general, the extinction coefficient can be given as

$$K_{e\lambda} = \frac{3f_v Q_{e\lambda}(\alpha, m)}{D} \tag{6}$$

where f_v is the particle volume fraction, and $Q_{e\lambda}$ is the extinction efficiency. The extinction efficiency in the Rayleigh regime is given by the following relation [15]:

$$Q_{e\lambda} = 4\alpha\,\text{Im}\left\{\frac{m^2-1}{m^2+2}\left[1 + \frac{\alpha^2}{15}\left(\frac{m^2-1}{m^2+2}\right)\frac{m^4+27m^2+38}{2m^2+3}\right]\right\} + \frac{8}{3}\alpha^4\left|\left(\frac{m^2-1}{m^2+2}\right)\right|^2 \tag{7a}$$

where the extinction efficiency ($Q_{e\lambda}$) term shown above contains two terms—the absorption efficiency ($Q_{a\lambda}$) and scattering efficiency ($Q_{s\lambda}$)—as shown below

$$Q_{a\lambda} = 4\alpha\,\text{Im}\left\{\frac{m^2-1}{m^2+2}\left[1 + \frac{\alpha^2}{15}\left(\frac{m^2-1}{m^2+2}\right)\frac{m^4+27m^2+38}{2m^2+3}\right]\right\} \tag{7b}$$

$$Q_{s\lambda} = \frac{8}{3}\alpha^4\left|\left(\frac{m^2-1}{m^2+2}\right)\right|^2 \tag{7c}$$

By examining Eq. (7*c*) it is evident that the scattering efficiency ($Q_{s\lambda}$) varies as the fourth power of particle size. In addition, it is found that absorption efficiency ($Q_{a\lambda}$) *predominantly* varies almost linearly with particle size. This is true even though there is a α^2 term inside the imaginary term of Eq. (7*b*) because $\alpha \ll 1$. This α^2 term does have a small influence which will become evident in Fig. 4 and will be discussed later in that section. Further, by substituting Eqs. (4) and (7*a*) into Eq. (6), the following expression for $K_{e\lambda}$ is obtained:

$$K_{e\lambda} = \frac{12\pi f_v}{\lambda}\text{Im}\left\{\frac{m^2-1}{m^2+2}\left[1 + \frac{\pi^2 D^2}{15\lambda^2}\left(\frac{m^2-1}{m^2+2}\right)\frac{m^4+27m^2+38}{2m^2+3}\right]\right\} + \frac{8\pi^4 D^3 f_v}{\lambda^4}\left|\left(\frac{m^2-1}{m^2+2}\right)\right|^2 \tag{8a}$$

where the extinction coefficient ($K_{e\lambda}$) term shown above contains two terms—the absorption coefficient ($K_{a\lambda}$) and scattering coefficient ($K_{s\lambda}$)—as shown below

$$K_{a\lambda} = \frac{12\pi f_v}{\lambda}\text{Im}\left\{\frac{m^2-1}{m^2+2}\left[1 + \frac{\pi^2 D^2}{15\lambda^2}\left(\frac{m^2-1}{m^2+2}\right)\frac{m^4+27m^2+38}{2m^2+3}\right]\right\} \tag{8b}$$

$$K_{s\lambda} = \frac{8\pi^4 D^3 f_v}{\lambda^4}\left|\left(\frac{m^2-1}{m^2+2}\right)\right|^2 \quad (8c)$$

Finally, using Eqs. (5) and (7*a*) the radiative properties of the nanofluid were evaluated. The net extinction caused by the nanofluid was obtained by adding the individual contributions from the nanoparticles (aluminum) as well as the base fluid (water). The intensity distribution within the solar collector was obtained using:

$$\frac{\partial I_\lambda}{\partial y} = -K_{e\lambda,\text{nanofluid}} I_\lambda = -(K_{a\lambda,\text{water}} + K_{e\lambda,\text{nanoparticles}}) I_\lambda \quad (8d)$$

where, $K_{a\lambda,\text{water}}$ and $K_{e\lambda,\text{nanoparticles}}$ are obtained from Eqs. (3) and (6) respectively. When the volume fraction of nanoparticles is low the contributions of nanoparticles and base fluid (water) could be added together as shown in Eq. (8*d*). This is because the present model assumes independent scattering, where the scattered radiations do not depend on one another and hence the intensities can be added. Once the intensity distributions were evaluated, the energy balance on the solar collector was performed and the temperature profile within it was obtained. In order to carry out these steps, some assumptions were made. The heat transfer model was considered as a steady-state two-dimensional case. Thus, the following energy balance equation was applied

$$k\frac{\partial^2 T}{\partial y^2} - \frac{\partial q_r}{\partial y} = \rho c_p U \frac{\partial T}{\partial x} \quad (9a)$$

where ρ is the density of the liquid film, c_p is the specific heat, U is the fluid velocity, k is the thermal conductivity, and q_r is the radiative heat flux defined as

$$q_r = \int_\lambda \int_\phi I_\lambda d\phi d\lambda \quad (9b)$$

The velocity profile was assumed to be uniform (i.e., slug flow), hence U is independent of x and y. The boundary condition at the top surface of the collector was considered as constant convective heat transfer, given by

$$Q_{\text{conv}} = h_{\text{conv}} A (T - T_{\text{amb}}) \quad (10)$$

while the boundary condition at the bottom was considered as adiabatic. The temperature of the fluid entering the solar collector was kept constant at a fixed value of $T_{\text{in}} = 35^\circ\text{C}$. Finally, the collector efficiency was evaluated by using the following relation [16]:

$$\eta = \frac{\text{useful gain}}{\text{available energy}} = \frac{\dot{m} c_p (\bar{T}_{\text{out}} - \bar{T}_{\text{in}})}{A G_T} \quad (11)$$

where $\dot{m}$ is the mass flow rate of the fluid flowing through the solar collector, T_{in} and T_{out} are the mean fluid inlet and outlet temperatures, respectively, A is the top cover area of the solar collector, and G_T is the solar flux incident on the solar collector.

3 Numerical Modeling

In order to solve the radiative transport equation (2) and the energy balance equation (9*a*), a finite difference technique was used. Accordingly, the spectral and spatial spaces were divided into uniform nodes of finite differences, as shown in Fig. 1. For example, the collector, which has a thickness, H, of 1.2 mm, was divided into a certain number of nodes, N_y(=1000), each having a thickness, dy, of 1.2 μm. Along the length of the collector (L = 1 m), the space was divided into N_x(=160) nodes, each having a length, dx, of 0.00625 m. Similarly the spectral space, which was considered in solving the radiative transport equation, was divided into uniform bands of 0.02 μm width. 150 such bands were considered in this model, which allowed the evaluation of the spectral radiative properties from a wavelength starting from near 0 μm up to 3 μm. Each of these intervals was chosen such that the iterations consistently gave convergent and stable solutions. Once the governing equations (2) and (9*a*) were discretized using the aforementioned technique, they were solved using the forward difference implicit method.

Table 1 Physical properties of water and aluminum at 25°C [19]

	Water	Aluminum
Density (ρ) (kg/m^3)	997	2700
Specific heat (c_p) (J kg^{-1} K^{-1})	4180	900
Thermal conductivity (k) (W m^{-1} K^{-1})	0.607	247

In order to apply the boundary conditions the heat flux at the bottom surface was taken as zero, although for radiative transfer that surface was considered to be transparent. The top cover (made of glass) was assumed to have a transmissivity (τ) of 0.9 [17]. At the top surface the heat loss was considered to be due to convection. The temperature of ambient air was taken as 25°C with a convective heat transfer coefficient (h_{conv}) of 6.43 W m^{-2} K^{-1}. This value was chosen to be equal to the overall heat transfer coefficient value in Ref. [17]. Likewise the value of incident solar flux (G_T=1000 W/m^2) was taken to be equal to the corresponding value in Ref. [17] to preserve compatibility and to provide a fair comparison of the nanofluid-based collector results to a flat-plate collector. The particle size (D) was taken as 5 nm, and the particle volume fraction was chosen as 0.8%, for the normal operating conditions. The fluid was assumed to be initially at a uniform temperature (35°C) and assumed to enter the collector at the same temperature (T_{in}=35°C). Table 1 shows the physical properties of water and aluminum that were used during these calculations. The optical properties of water and aluminum (such as n, κ) were obtained from Ref. [18].

4 Results and Discussion

This section begins by presenting the basic results obtained from the solar collector model under normal operating conditions. Later on, the influences of variations in several operating parameters, such as the particle size, particle volume fraction, and others, on the collector efficiency are discussed. Finally, the collector efficiency results for the present model are compared with those of a conventional flat-plate type collector using pure water as its working fluid.

Figure 2 shows the plot of spectral intensity (I_λ) as a function of the wavelength, at various depths (y) within the solar collector. The depth within the solar collector (y) has been normalized by the total depth (H) of the collector. As can be observed in this figure, the spectral intensity is the highest at the top (where y/H =0) and gradually reduces with depth. Since the nanofluid mixture has selective optical properties, the radiant intensity is selectively absorbed and scattered. For example, it can be seen from Fig. 2 that the largest attenuation in intensity takes place in the region of about 0.5–1 μm, where a large portion of the incident sunlight energy is present. As was mentioned previously in these calculations the atmospheric absorption by various constituent gases has been neglected, hence, no sharp troughs are visible in the spectral intensity distribution, which would have appeared otherwise. Figure 3 shows the temperature distribution as a function of the depth of the collector (y) and at various distances along the collector (x). Both these parameters were normalized using the collector depth (H) and collector length (L), respectively. This plot shows that, as expected, the temperature of the fluid increases as it flows through the collector. Moreover, the change in temperature is not uniform. The temperature increase is the highest for the top layers and decreases with depth. This result is consistent with those pre-

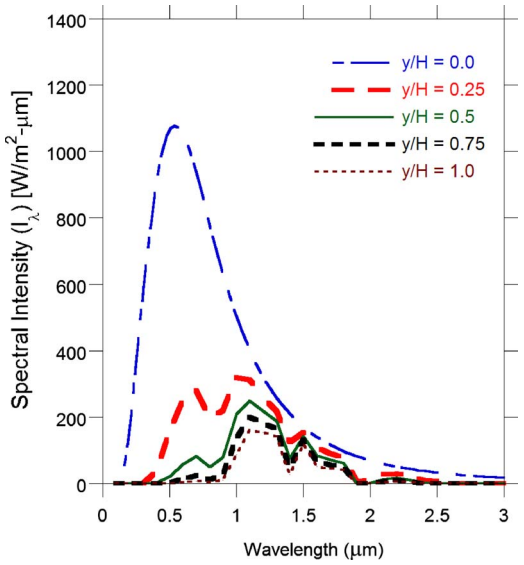

Fig. 2 Spectral radiant intensity within the solar collector at various depths (D=5 nm and f_v=0.8%)

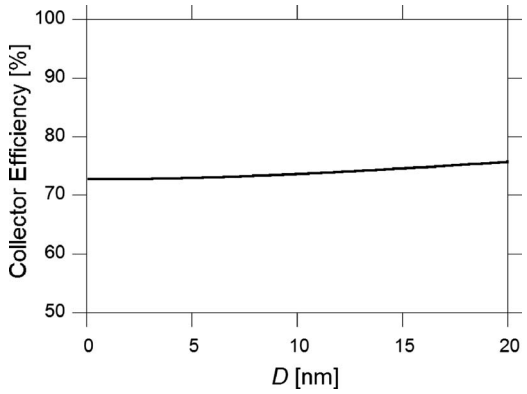

Fig. 4 Collector efficiency (Eq. (11)) as a function of the particle size (D) (f_v=0.8%)

sented in Fig. 2, which depict that the maximum attenuation in the spectral intensity occurs in the top layers, and decreases along the depth of the collector.

The variation in the collector efficiency, defined in Eq. (11), as a function of the particle size (D) is presented in Fig. 4. The particle sizes in these calculations were varied from 1 nm to 20 nm. The lower limit was chosen based on practical considerations, and the upper limit was chosen such that the Rayleigh regime approximation for the scattering calculations remained valid [15]. It was found that, with all other parameters (such as particle volume fraction, collector height, and collector length) being constant, the collector efficiency increased slightly with an increase in the particle size, as can be easily observed from Fig. 4. Under normal operating conditions, with D=5 nm and a particle volume fraction, f_v=0.8%, the collector efficiency was found to be about 73%.

The increase in collector efficiency with particle size, as observed in Fig. 4, can be explained as follows. When Eq. (7*a*) is substituted into Eq. (6) and solved for $K_{e\lambda}$, Eq. (8*a*) is obtained. Furthermore, as explained earlier, $K_{e\lambda}$ consists of two terms ($K_{a\lambda}$ and $K_{s\lambda}$), which are shown in Eqs. (8*b*) and (8*c*) respectively. These equations clearly show that scattering coefficient ($K_{s\lambda}$) varies as the third power of particle size (D^3). Since the particle size (D) is extremely small in the present calculations, this term becomes negligible. The absorption coefficient ($K_{a\lambda}$) on the other hand has a complicated expression, shown in Eq. (8*b*). However it can be seen that the expression for $K_{a\lambda}$ has a fixed part and another part which varies as D^2. It was verified in this study that the slightly increasing behavior of the curve seen in Fig. 4 is due to the D^2 term. Just as an exercise, if the D^2 term is removed from the expression given in Eq. (8*a*), the collector efficiency was found to be virtually constant and hence would be represented by a flat line in Fig. 4. To summarize, since D is extremely small in the present calculations the fixed term dominates and the term which varies as D^2 has a very small impact, which is evident in Fig. 4, and is manifested in the very gradual increase in the curve. Theoretically, it may be expected that at much higher particle sizes, the second term would eventually dominate and the efficiency would perhaps increase much more rapidly. However, as mentioned previously, above a certain particle size, the Rayleigh approximation would no longer be applicable and the simplified expression, given by Eqs. (7*a*) and (8*a*), would no longer be valid.

Figure 5 shows the variation in collector efficiency as a function of the particle volume fraction (f_v). The particle volume fraction was varied in the range 0.1% to about 5% in these calculations. As can be observed from this figure, the collector efficiency increases rapidly with volume fraction and tends to reach a maximum value of around 80% near the upper limit. This trend can be understood as follows. Increasing the particle volume fraction

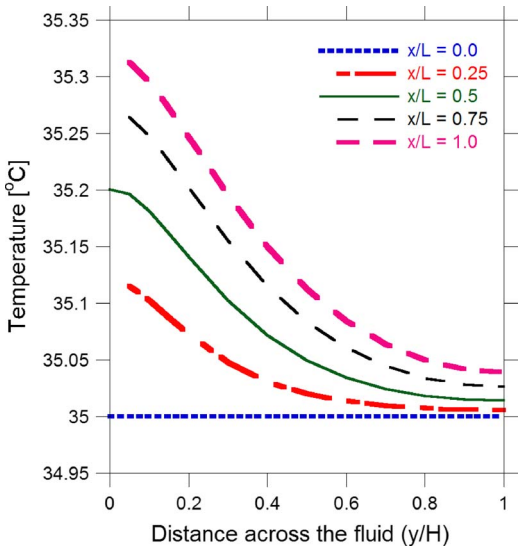

Fig. 3 Temperature distribution within the solar collector (D=5 nm and f_v=0.8%)

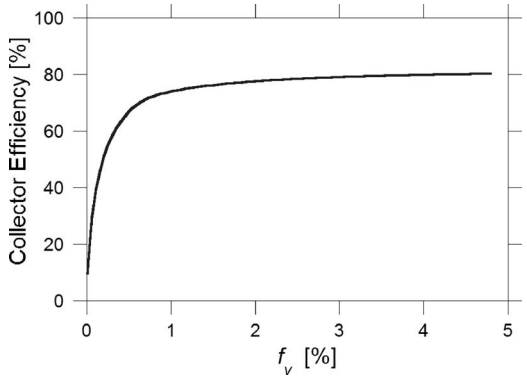

Fig. 5 Collector efficiency (Eq. (11)) as a function of the particle volume fraction (f_v) (D=5 nm)

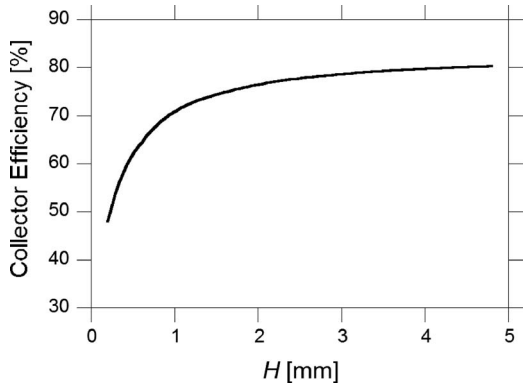

Fig. 6 Collector efficiency (Eq. (11)) as a function of the collector height (H) (D=5 nm and f_v=0.8%)

leads to a corresponding increase in attenuation of sunlight passing through the collector, and this, in turn, increases the collector efficiency. Since the attenuation varies exponentially with the extinction coefficient (and hence also with volume fraction, according to Eq. (6)), the efficiency initially increases very rapidly (at low volume fraction) and quickly reaches an asymptotic value (at higher volume fractions). This result also indicates that adding large amount of nanoparticles will be advantageous only up to a certain limit, beyond which the increase in efficiency would be miniscule. For the nanofluid considered here, consisting of water with 5 nm nanoparticles, that limit is $f_v \sim 2\%$.

Another important parameter which affects the performance of a solar collector is the transmissivity (τ) of the glass cover. Under ideal operating conditions the transmissivity of the glass cover is a constant (as a function of wavelength) and is easily determined for a known glass-cover material. However, in actual operating conditions it is also affected by conditions such as dust accumulation and wear-and-tear over time. It was observed that the collector efficiency increases almost linearly with an increase in the transmissivity. For example, the collector efficiency was about 55% for a glass-cover transmissivity of 0.7, and reaches about 74% for a glass-cover transmissivity of 0.9, which is the value used for most calculations.

The influence of the solar collector height (H) and length (L) on the collector efficiency are shown in Figs. 6 and 7, respectively. Under the normal operating conditions, the collector height and length were H=1.2 mm and L=1 m respectively. For these calculations, the collector height was varied from 0.2 mm to about 5 mm. The collector efficiency increases with collector height, and reaches an asymptotic value of about 80%. This phenomenon can

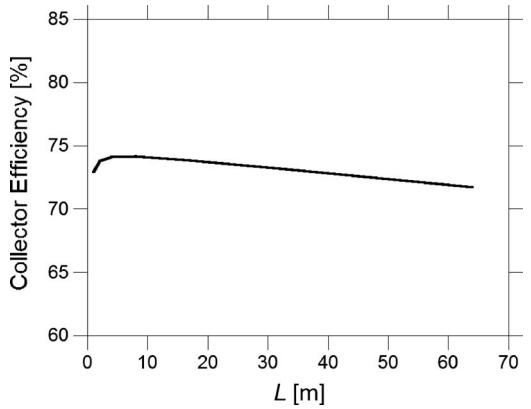

Fig. 7 Collector efficiency (Eq. (11)) as a function of the collector length (L) (D=5 nm and f_v=0.8%)

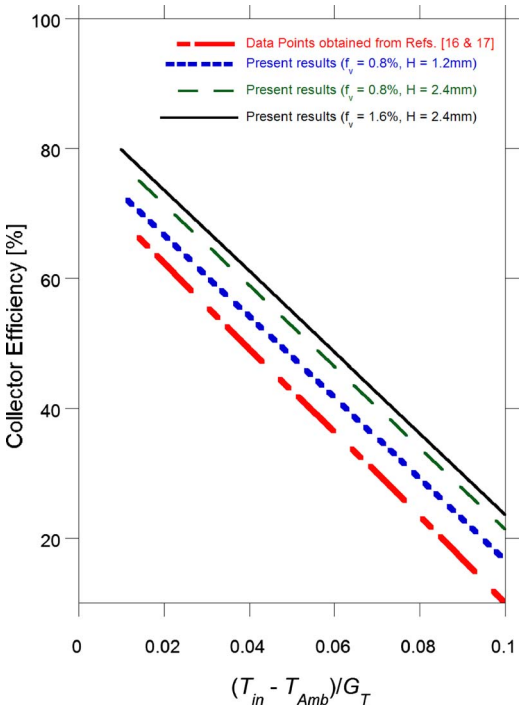

Fig. 8 Collector efficiency (Eq. (11)) as a function of the normalized fluid inlet temperature, $(T_{in}-T_{amb})/G_T$, at different values of fluid thickness (H) and particle volume fraction (f_v) (D=5 nm). Shown for comparison are results for a conventional flat-plate collector [16,17].

be explained as follows. Previously, it was shown (in Fig. 2) that the spectral intensity of the sunlight reduces as it travels through the fluid. Hence, for a solar collector with a greater depth, the amount of attenuation experienced by the sunlight will correspondingly be higher. This attenuation is caused because the solar energy is being absorbed directly by the nanofluid, which causes it to heat up. Therefore any attenuation in sunlight manifests in term of higher fluid temperatures and hence higher efficiencies. Moreover, the spectral intensity of the sunlight, as governed by Eq. (2), tends to attenuate in an exponential form, which is eventually manifested as an asymptotic-type curve in Fig. 6.

The influence of the collector length (L) on efficiency is given in Fig. 7. This plot shows that the efficiency initially increases with length and then gradually decays. Since the radiative energy decreases exponentially as the incident radiation passes through the collector, the topmost layers get heated the most. Simultaneously, heat is conducted to the underlying fluid layers, and some heat is lost via convection to the ambient. The relative magnitudes of these two modes of heat transfer vary along the length of the collector. At very small collector lengths the temperatures are relatively low and hence convective heat loses are not significant. However, as the length is increased, after a certain point the relatively higher temperatures of the top layers contribute to higher convective losses, and thus the efficiency tends to gradually decrease with further increases in length. Although the present results suggest that the influence of the overall length of the collector on the collector efficiency is relatively small, an optimum collector length can nevertheless be defined.

Finally, the collector efficiency of the DAC is compared with that of a conventional flat-plate type collector that uses pure water as its working fluid. These results are presented in Fig. 8, where the collector efficiency is plotted as a function of the inlet fluid temperature (T_{in}), given in normalized form as $(T_{in}-T_{amb})/G_T$. All the external operating parameters for these calculations are identical to those for the conventional flat-plate collector, in order to

perform a direct comparison of their efficiencies. As can be seen in this figure, the collector efficiency of the present model, under normal operating conditions, can be ~10% higher (on an absolute basis) than that of a typical flat-plate collector at almost all the operating points (both type of collectors being under similar conditions). The nanofluid-based DAC's efficiency is about 20% at high values of $(T_{in}-T_{amb})/G_T$, and increases to about 75% at low values of $(T_{in}-T_{amb})/G_T$. Moreover as demonstrated by the three different nanofluid-based DAC curves, it is possible to further increase the collector efficiency, with respect to the normal operating conditions, by manipulating the particle volume fraction (f_v) and the height of the collector (H), while keeping all the other parameters fixed. For example, when the height of the collector is doubled from 1.2 mm to 2.4 mm, an absolute gain in efficiency of about 5% is obtained. Moreover, if the particle volume fraction is doubled as well, from 0.8% to 1.6%, a corresponding absolute gain in efficiency of about 8% is obtained. Such increases in efficiency will potentially enable more effective use of solar heating devices for various purposes—cheaper air heating, water heating, and chemical processing. Additionally, in applications where high incident fluxes are used (such as those produced by large heliostat fields), a nanofluid-based DAC can achieve relatively higher temperatures, compared with a flat-plate type collector, due to lower heat losses.

5 Conclusion

A direct absorption solar collector was modeled numerically using a two-dimensional heat transfer analysis. A nanofluid—a mixture of water and aluminum nanoparticles—was used as the working fluid in the solar collector. The influences of various parameters, such as nanoparticle size and volume fraction, and collector geometry on the collector efficiency were studied, and finally the performance of this collector was compared with that of a conventional flat-plate type collector. The collector efficiency was found to increase with particle volume fraction (f_v), glass-cover transmissivity (τ), and the collector height (H). According to the present results, the particle size (D) and the length of the collector (L) did not significantly influence the collector efficiency. Finally, the results showed about 10% higher absolute efficiencies for the nanofluid-based direct absorption solar collector in comparison with conventional flat-plate type collectors that use pure water under similar operating conditions. Generally a DAC using nanofluids as the working fluid performs better than a flat-plate collector, however much better designed flat-plate collectors might be able to match or outperform a nanofluids based DAC under certain conditions.

Acknowledgment

The authors gratefully acknowledge the support of the National Science Foundation through a GOALI Award to Arizona State University and the Intel Corporation (Grant No. CTS-0353543). PEP acknowledges that this material was based on work supported by the National Science Foundation, while working at the Foundation.

Nomenclature

A = area (m^2)
c_o = speed of light in vacuum, $c_o=2.9979\times10^8$ m/s
c_p = specific heat (J kg^{-1} K^{-1})
D = mean particle diameter, $D=5\times10^{-9}$ m(=5 nm)
dx = length of a spatial node, $dx=0.00625$ m
dy = thickness of a spatial node, $dy=1.2$ μm
$d\lambda$ = spectral interval, $d\lambda=0.02$ μm
f_v = particle volume fraction, $f_v=0.8\%$
G_T = incident solar flux on the collector plane, $G_T=1000$ W/m^2
h = Planck constant, $h=6.6256\times10^{-34}$ J s
h_{conv} = convective heat transfer coefficient, $h_{conv}=6.43$ W m^{-2} K^{-1}
H = thickness of the solar collector, $H=1.2$ mm
I = intensity (W m^{-2} str^{-1} μm^{-1})
J = total number of spectral nodes, $J=150$
k = thermal conductivity (W m^{-1} K^{-1})
k_B = boltzmann constant, $k_B=1.38\times10^{-23}$ J/K
K = radiative coefficients (m^{-1})
L = length of the solar collector, $L=1$ m
m = complex refractive index, $m=n+i\kappa$
$\dot{m}$ = mass flow rate of the fluid flowing through the solar collector, $\dot{m}=1.2$ kg/s
n = index of refraction
N_x = total number of spatial nodes along the x-direction, $N_x=160$
N_y = total number of spatial nodes along the y-direction, $N_y=1000$
q = heat flux (W/m^2)
Q = radiative efficiency
T = temperature (°C)
U = fluid velocity, $U=1$ m/s
W = width of the solar collector, $W=1$ m
x,y = Cartesian coordinates

Greek Symbols

α = size parameter ($=\pi D/\lambda$)
η = collector efficiency (%)
κ = index of absorption
λ = wavelength (μm)
ρ = density (kg/m^3)
τ = transmissivity, $\tau=0.9$
ϕ = solid angle (str)

Subscripts

a = absorption
amb = ambient
b = blackbody
c = collector
conv = convection
e = extinction
in = inlet
out = outlet
r = radiative
s = scattering
λ = spectral

References

[1] Okujagu, C. U., and Adjepong, S. K., 1989, "Performance of a Simple Flat-Plate Collector at an Equatorial Location," Sol. Wind Technol., **6**, pp. 283–289.
[2] Minardi, J. E., and Chunag, H. N., 1975, "Performance of a Black Liquid Flat-Plate Solar Collector," Sol. Energy, **17**, pp. 179–183.
[3] Bertocchi, R., Karni, J., and Kribus, A., 2004, "Experimental Evaluation of a Non-Isothermal High Temperature Solar Particle Receiver," Energy, **29**, pp. 687–700.
[4] Miller, F. J., and Koenigsdorff, R. W., 2000, "Thermal Modeling of a Small-Particle Solar Central Receiver," ASME J. Sol. Energy Eng., **122**, pp. 23–29.
[5] Abdelrahman, M., Fumeaux, P., and Suter, P., 1979, "Study of Solid-Gas Suspension Used for Direct Absorption of Concentrated Solar Radiation," Sol. Energy, **22**, pp. 45–48.
[6] Kumar, S., and Tien, C. L., 1990, "Analysis of Combined Radiation and Convection in a Particulate Laden Liquid Film," ASME J. Sol. Energy Eng., **112**, pp. 293–300.
[7] Prasher, R. S., and Phelan, P. E., 2005, "Modeling of Radiative and Optical Behavior of Nanofluids Based on Multiple and Dependent Scattering Theories," ASME IMECE, Orlando, FL, Paper No. IMECE2005-80302.
[8] Prasher, R. S., 2005, "Modification of Planck Blackbody Emissive Power and Intensity in Particulate Media Due to Multiple and Dependent Scattering," ASME J. Heat Transfer, **127**, pp. 903–910.

[9] Prasher, R. S., Bhattacharya, P., and Phelan, P. E., 2005, "Thermal Conductivity of Nanoscale Colloidal Solutions (Nanofluids)," Phys. Rev. Lett., **94**, p. 025901.
[10] Bhattacharya, P., Saha, S. K., Yadav, A., Phelan, P. E., and Prasher, R. S., 2004, "Brownian Dynamics Simulation to Determine the Effective Thermal Conductivity of Nanofluids," J. Appl. Phys., **95**, pp. 6492–6494.
[11] Prasher, R. S., Bhattacharya, P., and Phelan, P. E., 2006, "Brownian-Motion-Based Convective-Conductive Model for the Effective Thermal Conductivity of Nanofluids," ASME J. Heat Transfer, **128**, pp. 588–595.
[12] Prasher, R. S., Phelan, P. E., and Bhattacharya, P., 2006, "Effect of Aggregation Kinetics on the Thermal Conductivity of Nanoscale Colloidal Solutions (Nanofluids)," Nano Lett., **6**, pp. 1529–1534.
[13] Krishnamurthy, S., Bhattacharya, P., and Phelan, P. E., 2006, "Enhanced Mass Transport in Nanofluids," Nano Lett., **6**, pp. 419–423.
[14] Phelan, P. E., Bhattacharya, P., and Prasher, R. S., 2005, "Nanofluids for Heat Transfer Applications," Annu. Rev. Heat Transfer, **14**, pp. 255–275.
[15] Bohren, C. F., and Huffman, D. R., 1983, *Absorption and Scattering of Light by Small Particles*, Wiley, New York.
[16] Duffie, J. A., and Beckman, W. A., 1980, *Solar Engineering of Thermal Processes*, Wiley, New York.
[17] Streed, E. R., Hill, J. E., Thomas, W. C., Dawson, A. G., and Wood, B. D., 1979, "Results and Analysis of a Round Robin Test Program for Liquid-Heating Flat-Plate Solar Collectors," Sol. Energy, **22**, pp. 235–249.
[18] Brewster, M. Q., 1992, *Thermal Radiative Transfer and Properties*, Wiley, New York.
[19] Cengel, Y. A., 2003, *Heat Transfer: A Practical Approach*, 2nd ed., McGraw Hill, New York.